First-principles study of structural, electronic, dynamical, and dielectric properties of zircon

G.-M. Rignanese and X. Gonze
Unité de Physico-Chimie et de Physique des Matériaux, Université Catholique de Louvain, 1 Place Croix du Sud, B-1348 Louvain-la-Neuve, Belgium

Alfredo Pasquarello
Institut Romand de Recherche Numérique en Physique des Matériaux (IRRMA), Ecole Polytechnique Fédérale de Lausanne (EPFL), PPH-Ecublens, CH-1015 Lausanne, Switzerland

(Received 29 August 2000; published 20 February 2001)

We investigate structural, electronic, dynamical, and dielectric properties of zircon ($ZrSiO_4$) within density-functional theory. The atomic structure is fully relaxed and the structural parameters are found to differ by less than 1.5% from the experimental data. The associated electronic band structure and density of states are also presented. Using density-functional perturbation theory, we obtain the phonon frequencies at the center of the Brillouin zone, the Born effective charge tensors, and the dielectric permittivity tensors. The calculated phonon frequencies agree with the infrared and Raman experimental values (rms relative deviations of 2.5%) when available, while the silent modes are predicted to range between 119.6 and 943.3 cm^{-1}. We compute the Born effective charge tensors, that are found to be quite anisotropic. The electronic and static dielectric permittivity are analyzed in detail. Their difference is mostly due to the lowest infrared-active mode, whose eigenvector corresponds to a distortion of the SiO_4 tetrahedra with a displacement of Zr and O atoms in opposite directions.

DOI: 10.1103/PhysRevB.63.104305 PACS number(s): 63.20.−e, 71.20.−b, 77.22.−d

I. INTRODUCTION

Zircon ($ZrSiO_4$) is a mineral of widespread geological occurrence found in igneous rocks and sediments. It is used as a gemstone, because of its good optical quality, and resistance to chemical attack. In the Earth's crust, zircon is a host mineral for the radioactive elements uranium and thorium, and therefore a natural candidate for usage as a nuclear waste storage material.

More recently, the Zr-Si-O system has drawn considerable attention in the quest for an alternative high-permittivity (high-ϵ) material to conventional SiO_2 as the gate dielectric in metal-oxide-semiconductor (MOS) devices.[1] Indeed, the metal oxide ZrO_2 as well as $ZrSiO_4$ in the form of amorphous films are stable in direct contact with Si up to high temperature, which is highly desirable to avoid the degradation of the interface properties by formation of a low-ϵ interfacial layer. The pure oxide ZrO_2 presents some potential concerns:[1] it tends to crystallize at low temperature, it is an ionic conductor, and the heterointerface formed between the Si channel and ZrO_2 may degrade the electron channel mobility in transistors. On the contrary, amorphous silicates of the type $ZrSi_xO_y$ appear as very promising candidates for replacing SiO_2. In fact, the Zr-Si-O phase diagram presents a large phase field of stable $ZrSi_xO_y$ and the static permittivity ϵ_0 increases continuously with the amount of Zr incorporated into the silicate film.[2] For crystalline $ZrSiO_4$ (zircon), values of ϵ_0 ranging from 10.69 (Ref. 3) to 12.6 (Ref. 4) are reported, which is consistent with the fact that its structure is comprised of SiO_2 ($\epsilon_0=3.9$) and ZrO_2 ($\epsilon_0=25$) components.

In order to be able to control this process, it is highly desirable to develop an understanding of how the permittivity of $ZrSi_xO_y$ is affected by its microstructure. In this work, we take the first step towards this goal by establishing the accuracy of first-principles approaches for describing the structural, electronic, vibrational, and dielectric properties of such materials. To this end, we here consider zircon (crystalline $ZrSiO_4$), which presents all the principal bonding features occurring in $ZrSi_xO_y$ silicate films. Using density-functional theory, we first study the ground-state properties of this material. The relaxed atomic structure is found in excellent agreement with the experimental one. The electronic band structure and density of states are also given. We use density-functional perturbation theory to compute the phonon frequencies at the Γ point of the Brillouin zone, the Born effective charge tensors, and the dielectric permittivity tensors of $ZrSiO_4$. We find very good agreement between calculated and measured phonon frequencies, and predict the frequencies of seven modes (five silent modes—inactive for both infrared (IR) and Raman techniques—and two Raman-active modes that were not observed in experiments). The Born effective charge tensors are quite anisotropic and, for some directions, larger than the nominal ionic charges. This phenomenon, which has already been observed in various oxides (see Ref. 5 and references therein) is called ''anomalous effective charge.'' It indicates a mixed covalent-ionic character of the Zr-O bonding. The agreement with experiments is also rather good for the electronic and static dielectric permittivity constants. The latter is decomposed into its electronic component and the individual contributions of the IR-active modes. Four IR-active E_u modes contribute to the static dielectric constant in the plane perpendicular to the tetragonal axis, while three IR-active A_{2u} modes contribute to it along the tetragonal axis. In both cases, the lowest of these modes account for more than 60% of the difference between the electronic and static dielectric constant. We examine these lowest frequency A_{2u} and E_u modes, and show that, unlike assumed in an early analysis,[6] the SiO_4 group is substantially deformed. This supports the above-mentioned

mixed ionic-covalent Zr-O bonding.

This paper is organized as follows. In Sec. II, we discuss the ground-state properties of zircon. We compare our calculated structural parameters with the experimental ones and those from other theoretical calculations. In this section, we also give the electronic band structure and density of states of $ZrSiO_4$. In Sec. III, we present the calculated linear-response functions: the Born effective charge tensors, the phonon frequencies at the Γ point of the Brillouin zone, and the dielectric permittivity tensors. This section also contains the above-mentioned analysis of the difference between electronic and static dielectric constants. Finally, our results are summarized in Sec. IV.

II. GROUND-STATE PROPERTIES OF ZIRCON

A. Technical details

Our calculations are performed within the local density approximation (LDA) to density-functional theory,[7,8] as implemented in the ABINIT package, developed by the authors and collaborators.[9] The exchange-correlation energy is evaluated using Perdew-Wang's parametrization[10] of Ceperley-Alder electron-gas data.[11] The all-electron potentials are replaced by extended norm-conserving, highly transferable pseudopotentials,[12] with Zr($4s,4p,4d,5s$), Si($3s,3p$), and O($2s,2p$) levels treated as valence states. The wave functions are expanded in plane waves up to a kinetic energy cutoff of 30 Ha. The Brillouin zone is sampled by a $4\times4\times4$ Monkhorst-Pack[13] mesh of k points. Both kinetic energy cutoff and k-point sampling prove largely sufficient for the accuracy required in the present study.[14]

B. Atomic structure of zircon

We first determine the ground-state structural parameters of $ZrSiO_4$. Zircon has a conventional unit cell which is body-centered tetragonal (space group $I4_1/amd$, No. 141) and contains four formula units of $ZrSiO_4$. The experimental values of the lattice constants a and c taken from Ref. 15 are reported in Table I. A primitive cell containing only two formula units can be defined. The structure of zircon may be viewed as consisting of $(SiO_4)^{4-}$ anions and Zr^{4+} cations, as illustrated in Fig. 1 of Ref. 6. This is consistent with the larger bond length (about 25%) of Zr-O compared to Si-O bond (see Table I). Alternatively, as presented in Fig. 1 of Ref. 16, a different view may be adopted in which $ZrSiO_4$ consists of alternating (discrete) SiO_4 tetrahedra and ZrO_8 units, sharing edges to form chains parallel to the c direction. Note that in these ZrO_8 units four O atoms are closer to the Zr atom than the four other ones (6% difference in the Zr-O bond length). The positions of the Zr and Si atoms are imposed by symmetry: they are located at $(0,\frac{3}{4},\frac{1}{8})$ and $(0,\frac{1}{4},\frac{3}{8})$ on the $4a$ and $4b$ Wyckoff sites, respectively. The O atoms occupy the $16h$ Wyckoff sites $(0,u,v)$, where u and v are internal parameters.

Table I summarizes the results obtained after structural and atomic relaxation. The calculated lattice constants a and c, as well as the internal parameters u and v are found to be in excellent agreement with their corresponding experimental values.[15] Interatomic distances and angles are within one or two percent of the experimental values, and also agree at that level with the results from a previous first-principles study.[17] This is largely sufficient to allow the further study of dynamical and dielectric properties.

TABLE I. Calculated structural parameters of $ZrSiO_4$ compared to experimental values (Ref. 15). The length unit is the Å.

	Theory		Experiment
	This work	From Ref. 17	
Lattice constants			
a	6.54		6.61
c	5.92		6.00
Volume			
V	127	129	131
Internal parameters			
u	0.0645		0.0646
v	0.1945		0.1967
Interatomic distances			
Si-O	1.61	1.63	1.62
Zr-O	2.10	2.11	2.13
	2.24	2.26	2.27
Bond angles			
O-Si-O	97°	96°	97°
	116°	117°	116°

C. Electronic structure of zircon

In Fig. 1, we present the calculated electronic density of states (DOS) and the electronic band structure for several directions in the Brillouin zone. For the nomenclature of points and lines in the Brillouin zone, see Ref. 18. We clearly distinguish four group of valence bands, the three lowest of which have a rather small dispersion, indicative of a weak hybridization: the DOS exhibits a very sharp peak at

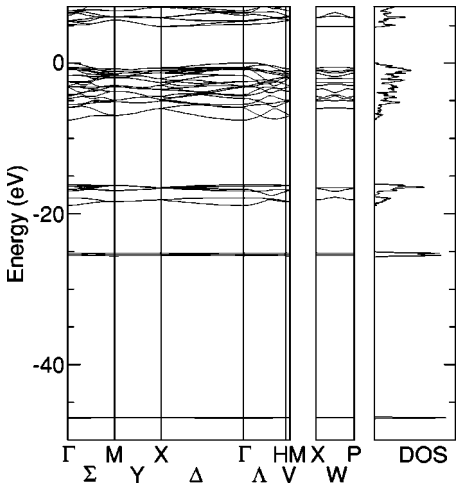

FIG. 1. Electronic band structure and density of states for $ZrSiO_4$. The Fermi level has been aligned to the top of the valence band.

TABLE II. Calculated Born effective charge tensors for Zr, Si, and O atoms in zircon. For Zr and Si atoms, the tensors are diagonal and only the principal elements are given. For O atoms, the full tensor is reported as well as the principal elements of its symmetric part, given between brackets.

Z^*_{Zr}	$(+5.41 \quad +5.41 \quad +4.63)$	
Z^*_{Si}	$(+3.25 \quad +3.25 \quad +4.42)$	
Z^*_O	$\begin{pmatrix} -1.15 & 0 & 0 \\ 0 & -3.17 & -0.16 \\ 0 & -0.34 & -2.25 \end{pmatrix}$	$\begin{bmatrix} -1.15 \\ -3.24 \\ -2.16 \end{bmatrix}$

-47.1 eV attributed to the Zr $4s$ states, corresponding to two flat bands; the peak at -25.5 eV is related to the Zr $4p$ states (six bands); the O $2s$ peak is located between -18.0 and -16.2 eV (eight bands). By contrast, the fourth group (24 bands), has a much wider spread of 8 eV : these states have mainly an O $2p$ character with some mixing of Si and Zr orbitals. This mixed covalent-ionic bonding of $ZrSiO_4$, appearing in this group of valence bands, is to be kept in mind for the interpretation of Born effective charge tensors.

III. LINEAR RESPONSE FUNCTIONS

A. Technical details

Linear response properties such as the Born effective charge tensors or the phonon frequencies are obtained as second-order derivatives of the total energy with respect to an external electric field or to atomic displacements. These second-order derivatives are calculated within a variational approach to density-functional perturbation theory.[9,19–21] The calculation of these quantities is a specific feature of the ABINIT package. We used the same parameters as for the calculation of the ground-state properties. We also performed tests which proved the associated numerical accuracy to be excellent.

B. Born effective charge tensors

We first compute the Born effective charge tensors ($Z^*_{ij,\tau}$). They are defined as the force in the direction i on the atom τ due to an homogeneous unitary electric field along the direction j, or equivalently, as the induced polarization of the solid along the direction i by a unit displacement in the direction j of the atomic sublattice.

In the zircon structure, the local site symmetry of Zr and Si atoms is rather high ($\bar{4}m2$). The Born effective charge tensors of Zr and Si atoms are diagonal and have only two independent components: along and perpendicular to the tetragonal axis, $Z^*_\parallel$ and $Z^*_\perp$, respectively. The Born effective charge tensors of Zr and Si atoms are reported in Table II.

We note that $Z^*_\perp$ for Zr is anomalously large compared to the nominal ionic charge of the zirconium ion $Z=+4$. A similar behavior was also observed in the case of $PbZrO_3$ (Ref. 22) and of cubic-ZrO_2 (Ref. 23). A detailed analysis of the physics of Born effective charges in the case of perovskite ferroelectrics (like $PbZrO_3$) ascribed this effect to a mixed covalent-ionic bonding.[5] In the section dealing with the electronic structure, we have seen the presence of Zr-O $2p$ hybridization. Thus the physical interpretation of this phenomenon is likely similar to the case of perovskite ferroelectrics. The other component of the zirconium Born effective charge tensor ($Z^*_\parallel$) is also larger than the nominal ionic charge, although the effect is not as pronounced. For the silicon atom, there are also some (weaker) deviations with respect to the nominal value ($Z=+4$), one component being slightly larger, and one being definitely lower. These are not very different to those observed in tetrahedrally bonded silica polymorphs, like quartz,[19] in which each O atom is strongly bonded to two Si atoms, or in the more compact polymorph of silica, stishovite,[24] in which each O atom has three close Si neighbors.

The local site symmetry of the O atoms has only a mirror plane. As a consequence, the Born effective charge tensor of O atoms is not diagonal, and depends on five independent quantities. We will examine the one for the O atom located at $(0,u,v)$, which has been reported in Table II. The Born effective charge tensors of the other oxygen atoms can be obtained using the symmetry operations. For this particular atom, the mirror plane is perpendicular to x. Note that Z^*_{yz} and Z^*_{zy} are different, but rather small, making the Born effective charge tensor almost diagonal. They appear in the mirror plane, where one O-Si bond and two O-Zr bonds (one long and one short) are present. One can compute the projection of the Born effective charge on these directions: for the O-Si bond, the projection is -2.29, while it is -3.23 for the shorter O-Zr bond, and -3.02 for the longer Zr-O bond. In this plane, the magnitude of Born effective charge components is larger than the nominal ionic charge of oxygen ($Z=-2$). In another approach to the characterization of the anisotropy of this tensor, one might select its symmetric part, and diagonalize it. The principal values are given in Table II and the principal direction associated to the largest principal value forms an angle of 14.2° with to the y axis. Both analysis give the same type of anisotropy.

Such a strong anisotropy of the Born effective charge tensor for O atoms, with one component with magnitude much smaller than 2 and much smaller than the two others, was already observed in SiO_2-stishovite[24] and TiO_2-rutile.[25] By contrast, in tetrahedrally bonded silicas, there are *two* components with magnitudes much smaller than 2. Thus, at the level of the Born effective charges, the ionic-covalent bonding of O atoms to Zr and Si atoms in $ZrSiO_4$ is closer to stishovite than to quartz, in agreement with a naive bond-counting argument. Models of $ZrSi_xO_y$ should take into account this difference, and might be classified according to the anisotropy of the O Born effective charges. With a small content of Zr, one could expect that the quartzlike behavior will dominate, while for Zr atomic fractions closer to that of zircon, the stishovitelike behavior will become stronger.

C. Phonon frequencies at the Γ point

We also compute the phonon frequencies at the Γ point of the Brillouin zone. Because of the nonvanishing components

TABLE III. Fundamental frequencies of zircon (in cm^{-1}) with their symmetry assignments. The experimental values are taken from Ref. 6 (first column), Ref. 3 (for A_{2u} mode in the second column), and Ref. 28 (for E_u mode in the second column).

Mode	This work	Experiment	
Raman			
$A_{1g}(1)$	442.0	439	
$A_{1g}(2)$	971.4	974	
$B_{1g}(1)$	225.4	214	
$B_{1g}(2)$	396.9	393	
$B_{1g}(3)$	631.7		
$B_{1g}(4)$	1016.7	1008	
B_{2g}	251.8	266	
$E_g(1)$	194.3	201	
$E_g(2)$	224.7	225	
$E_g(3)$	375.4	357	
$E_g(4)$	536.0	547	
$E_g(5)$	922.6		
Infrared			
A_{2u} (TO1)	347.8	338	339
A_{2u} (LO1)	475.9	480	478
A_{2u} (TO2)	601.2	608	605.7
A_{2u} (LO2)	646.0	647	641.5
A_{2u} (TO3)	979.9	989	977
A_{2u} (LO3)	1096.2	1108	1100
E_u (TO1)	285.2	287	281
E_u (LO1)	340.6	352	354
E_u (TO2)	383.0	389	381
E_u (LO2)	420.2	419	417
E_u (TO3)	422.2	430	429
E_u (LO3)	466.4	471	468
E_u (TO4)	867.4	885	871
E_u (LO4)	1028.6	1035	1034
Silent			
B_{1u}	119.6		
A_{2g}	241.7		
A_{1u}	392.3		
$B_{2u}(1)$	566.4		
$B_{2u}(2)$	943.3		

of the Born effective charge tensors, the dipole-dipole interaction has been properly included in the calculation of the interatomic force constants.[21,26,27] In particular, the dipole-dipole contribution is found to be responsible for the splitting between the longitudinal and transverse optic (LO and TO, respectively) modes E_u (perpendicular to c) and A_{2u} (parallel to c) at the Γ point.

In Table III, the calculated phonon frequencies are compared with experimental values.[3,6,28] Overall, the agreement is excellent, with a rms absolute deviation of 9.4 cm^{-1}, and a rms relative deviation of 2.5%. We obtain two Raman active modes at 631.7 cm^{-1} $[B_{1g}(3)]$ and at 922.6 cm^{-1} $[E_g(5)]$, that could not be detected experimentally. We also obtain silent modes, inactive for both IR and Raman experiments. They are found to range from 119.6 to 943.3 cm^{-1}. Two of these (B_{1u} and A_{2g}) are very soft, and correspond, in a first approximation, to vibration modes of zircon in which the SiO_4 tetrahedra rotate as a unit[6] (in the u and g modes the tetrahedra move with opposite phases).

TABLE IV. Electronic and static dielectric tensors of zircon. The contributions of the different phonon modes to the static dielectric tensor are also indicated. The tensors are diagonal and have different components parallel ($\|$) and perpendicular ($\perp$) to the c axis. The phonon mode contributions to $\epsilon_0^{\|}$ come from the three IR-active A_{2u} modes, while the contributions to $\epsilon_0^{\perp}$ come from the four IR-active E_u modes. The experimental values, in parentheses, are taken from Ref. 3 for the parallel components (values at 295 K), and from Ref. 28 for the perpendicular components.

	$\|$	$\perp$
ϵ_∞	4.26(3.8)	4.06(3.5)
$\Delta\epsilon_1$	5.90(5.75)	5.16(5.70)
$\Delta\epsilon_2$	0.52(0.36)	1.31(0.60)
$\Delta\epsilon_3$	0.85(0.78)	0.05(0.15)
$\Delta\epsilon_4$		1.38(1.20)
ϵ_0	11.53(10.69)	11.96(11.25)

On the basis of the close correspondence between our results and experimental data for IR-active and Raman-active modes, we are able to shed light on some delicate issues related to the interpretation of experimental results and the corresponding symmetry assignment.

Indeed, our calculations do not give any frequency of E_g symmetry close to the frequency of 1008 cm^{-1} experimentally observed by Dawson *et al.*[6] This lends support to their interpretation, which suggested that this line does not result from the perfect crystal, but rather from some crystal misorientation or imperfection. By contrast, as mentioned previously, we identify an E_g mode at 922.6 cm^{-1}.

Furthermore, we propose that the weak band found in experiments at 547 cm^{-1} should not be interpreted as a difference band between lines at 989 cm^{-1} (A_{2u} symmetry) and at 439 cm^{-1} (A_{1g} symmetry),[6] but rather as the frequency of a real eigenmode. In fact, we do find a phonon frequency at 536 cm^{-1} of E_g symmetry, quite close to this weak band (547 cm^{-1}). We have taken this reassignment into account in Table III.

D. Dielectric permittivity tensors

In this section, we present the electronic (ϵ_∞) and static (ϵ_0) permittivity tensors. Due to the symmetry of the zircon crystal, these have two independent components $\epsilon_\|$ and $\epsilon_\perp$ along and perpendicular to the c axis, respectively. The values of ϵ_∞ and ϵ_0 are compared with experimental data in Table IV: the theoretical values are larger than the experimental ones by about 10%, as often found in the LDA to the density-functional theory.

This problem has been widely discussed in the literature. The currently accepted view[29–31] is that a dependence on the polarization should be present in the exchange-correlation functional (leading to a density-polarization functional theory). However, no polarization dependence is present in

LDA, nor in other widely used approximations like the generalized-gradient approximation.[32] In view of practical calculations of the dielectric tensor, the LDA formalism can be modified somehow by adding a scissor operator.[33] The improvement is systematic for small-gap material, but not for large-gap materials.[34] This scissor operator approach is not well justified theoretically, although it bears an interesting relationship[29] with the well-known band-gap problem of density-functional theory.[35,36] In the present case, we find that the agreement with experiment is sufficiently good to proceed further in the analysis of the dielectric tensor. At this stage, we have all the ingredients to make such an analysis: we can rely not only on the frequencies of the IR-active modes, but also on the corresponding eigendisplacements and Born effective charges.

The static dielectric tensor can be decomposed in the contributions of different modes as follows (see Ref. 37; we follow the notations of Ref. 21):

$$\epsilon^0_{\alpha\beta}(\omega)=\epsilon^\infty_{\alpha\beta}+\sum_m \Delta\epsilon_{m,\alpha\beta}=\epsilon^\infty_{\alpha\beta}+\frac{4\pi}{\Omega_0}\sum_m \frac{S_{m,\alpha\beta}}{\omega_m^2}, \quad (1)$$

where Ω_0 is the volume of the primitive unit cell. $S_{m,\alpha\beta}$ is the mode-oscillator strength, related to the eigendisplacements $U_m(\kappa\alpha)$ and Born effective charge tensors by

$$S_{m,\alpha\beta}=\left(\sum_{\kappa\alpha'} Z^*_{\kappa,\alpha\alpha'}U^*_m(\kappa\alpha')\right)\left(\sum_{\kappa'\beta'} Z^*_{\kappa',\beta\beta'}U_m(\kappa'\beta')\right). \quad (2)$$

Displacements are normalized thanks to the condition

$$\sum_{\kappa\beta} M_\kappa[U_m(\kappa\beta)]^*U_n(\kappa\beta)=\delta_{mn}, \quad (3)$$

where M_κ is the mass of the ion κ.

The contribution of the individual modes $\Delta\epsilon_m$ to the static dielectric constant are presented in Table IV. The largest contribution comes from the lowest frequency mode.

In parallel to this decomposition of the static dielectric tensor, one can define a mode-effective charge vector:

$$Z^*_{m,\alpha}=\frac{\sum_{\kappa\beta} Z^*_{\kappa,\alpha\beta}U_m(\kappa\beta)}{\left[\sum_{\kappa\beta} U^*_m(\kappa\beta)U_m(\kappa\beta)\right]^{1/2}}. \quad (4)$$

In Table V, we present for each IR-active mode, the magnitude of its mode-effective charge vectors (this vector is parallel and perpendicular to the tetragonal axis for A_{2u} and E_u modes, respectively), as well as the relevant component of the oscillator strength tensor (the parallel-parallel component for A_{2u} modes, and the perpendicular-perpendicular component for E_u modes). In this table, we also compare the calculated mode-oscillator strengths with the experimental values. The good agreement that is found validates our analysis of the various contribution to the static dielectric constant.

For each symmetry representation (A_{2u} and E_u), the lowest and highest frequency mode exhibit the largest effective charges and the largest oscillator strengths. Despite their similar oscillator strengths, the modes of lowest frequency contribute much more to the static dielectric constant than the modes of highest frequency, the frequency factor in Eq. (1) playing a crucial role. The second lowest frequency modes are moderately strong, while the third E_u mode has a negligible IR activity.

TABLE V. Components of mode-effective charge vectors Z^*_m and oscillator strength tensor S_m for each of the IR-active modes. The experimental values of S_m, in parentheses, are taken from Ref. 3 for the A_{2u} modes and Ref. 28 for the E_u modes. The description of the vectors and the tensors structures corresponding to the two types of modes are given in the text. The components of the mode-effective charge vectors are given in atomic unit, that is minus the electronic charge. The oscillator strengths are presented in 10^{-4} atomic unit (1 a.u.$=0.342\,036$ m^3/s^2). The first-order approximation to the LO frequencies $\omega^{(1)}_m$ and to the LO-TO splitting $\Delta\omega^{(1)}_m$ are also given with the full LO-TO splitting $\Delta\omega_m$ (in cm^{-1}).

	Z^*_m	S_m	$\omega^{(1)}_m$	$\Delta\omega^{(1)}_m$	$\Delta\omega_m$
$A_{2u}(1)$	7.68	10.06(9.31)	546.1	198.3	128.1
$A_{2u}(2)$	2.76	2.65(1.86)	636.7	35.5	44.8
$A_{2u}(3)$	6.70	11.50(10.49)	1073.1	93.2	116.3
$E_u(1)$	6.79	5.92(6.34)	431.7	146.5	55.4
$E_u(2)$	3.51	2.71(1.23)	440.5	57.5	37.2
$E_u(3)$	0.28	0.13(0.39)	424.7	2.5	44.2
$E_u(4)$	7.37	14.63(12.83)	1004.6	137.2	161.2

Based on symmetry considerations and a crystal field analysis of the vibrations of $(SiO_4)^{4-}$ units, it was assumed in Ref. 6 that these two lowest IR-active modes correspond to opposite displacement of rigid SiO_4 groups against Zr atoms. The eigendisplacements that we obtain for these modes deviate significantly from this picture. The analysis of the A_{2u} eigenvector is rather easy: the Zr atoms move by -1.136 (arbitrary units) in the z direction, the Si atoms move by 0.429 in the z direction, and for the O atom located in $(0,u,v)$, the displacement is $(0,-0.563,1.429)$. Other O displacements can be found by symmetry (the z displacement being the same for all atoms). Clearly, the SiO_4 group does not move as a rigid building block. Along the z direction, the center of gravity of the four O ions moves in an opposite direction with respect to the motion of the Zr atom, with displacements of similar magnitude, while the Si atom displacement is more than twice smaller. The distortion of the O tetrahedra is also significant. Thus we obtain a picture which is rather different from the one of Fig. 3(b) in Ref. 6. This is also to be linked to the mixed ionic-covalent bonding between Zr and O.

From the mode-oscillator $S_{m,\alpha\beta}$, it is also possible to gain insight on the mixing of the eigenvectors of the dynamical matrix when going from TO to LO modes. In general, the eigenvectors of the dynamical matrix for $\mathbf{q}\rightarrow 0$ will not be identical to those for $\mathbf{q}=0$. Sometimes, symmetry constraints will be sufficient to guarantee that some of the eigendisplacements are identical, even if the eigenfrequencies are different. In this case, the following relationship holds that links LO and TO modes along the wave vector q_α [see Eq. (62) of Ref. 21]:

$$\Delta\omega_m = \left(\omega_m^2(\mathrm{TO}) + \frac{4\pi}{\Omega_0} \frac{\sum_{\alpha\beta} q_\alpha S_{m,\alpha\beta} q_\beta}{\sum_{\alpha\beta} q_\alpha \epsilon^\infty_{\alpha\beta} q_\beta} \right)^{1/2} - \omega_m(\mathrm{TO}). \tag{5}$$

More generally, this equation can be seen as the first-order approximation for the LO-TO splitting $\Delta\omega_m^{(1)}$. The calculated values are presented in Table V, together with the full LO-TO splittings $\Delta\omega_m$ derived from Table III. The differences between $\Delta\omega_m^{(1)}$ and $\Delta\omega_m$ indicate the occurrence of eigenvectors modifications. For the A_{2u} modes, there is a qualitative agreement, showing only moderate mixing of the eigenvectors when going from the TO to the LO case: the LO and TO modes of same index have a sizable overlap. This is also the case for the highest E_u mode, for which the agreement is within 20%. This mode is rather well separated from the other E_u modes, and a weak mixing is expected. By contrast, the three other E_u modes are strongly hybridized when going from the TO to LO case: the first-order approximation to the LO frequencies $\omega_m^{(1)}$, which are also provided in Table V, are roughly the same for these three modes (less than 16 cm^{-1} difference). This coincidence stems from the fact that for these three modes the oscillator strength decreases with increasing TO frequency. Consequently, while the TO frequencies are well separated, the first-order approximation to LO frequencies are close to each other.

IV. CONCLUSION

We have investigated the structural, electronic, dynamical, and dielectric properties of zircon (crystalline $ZrSiO_4$) within density-functional theory. The parameters of the relaxed atomic structure are found to be in very good agreement with experimental ones (at most 1.5% discrepancy). We have also calculated the electronic band structure and density of states in which the contributions from Zr $4s$ and $4p$, and O $2s$ and $2p$ are clearly distinguishable, although the spread of the latter indicates hybridization with Zr and Si atomic orbitals. The phonon frequencies at the center of the Brillouin zone, the Born effective charge tensors, and the dielectric permittivity tensors have been obtained using density-functional perturbation theory. We have found an excellent agreement between the calculated phonon frequencies and their corresponding experimental values (rms relative deviation of 2.5%) when available. The frequencies of two Raman-active modes, which have remained undetected in experiments, were determined (631.7 and 922.6 cm^{-1}). Silent modes have been found between 119.6 and 943.3 cm^{-1}. The Born effective charge tensors are quite anisotropic. For some directions, the Born effective charges are larger than the nominal ionic charge indicating a mixed covalent-ionic bonding between Zr and O. The anisotropy of the O Born effective charges has been proposed as a criterion to classify future models of $ZrSi_xO_y$. The electronic and static dielectric permittivity constants have been computed, and a detailed analysis of the contribution of the different vibrational modes has been performed, including computation of mode-effective charges and oscillator strengths. It is observed, for both the direction parallel to the tetragonal axis and the direction perpendicular to it, that a single mode contributes to more than 60% of the ionic contribution, in agreement with experimental data. Previously, this mode was thought to originate from an opposite displacement of Zr against SiO_4 rigid units. Our first-principle approach allows us to obtain the corresponding eigenvectors, showing clearly that the distortion of the SiO_4 tetrahedron is substantial, and that the displacement is better characterized as opposing Zr and O atoms, while the displacement of Si atoms is more than twice smaller than those of other species.

This work also demonstrates that first-principles approaches based on density-functional theory provide an accurate description of both the structure and the dielectric response functions of zircon. In previous investigations, a similar good description was obtained for α quartz[19] and cubic ZrO_2 (Ref. 23). This therefore suggests that density-functional approaches are particularly suited for studying the structure and the permittivity in amorphous silicate $ZrSi_xO_y$ films with compositions intermediate between those of α quartz and zircon. A better understanding of how the permittivity of $ZrSi_xO_y$ films relates to their underlying microstructure is highly desirable in relation with the search for alternative gate dielectrics in Si-based electronic devices.[1]

ACKNOWLEDGMENTS

The authors acknowledge interesting discussions with G. D. Wilk. G.-M.R. was supported by the Belgian Program on Interuniversity Attraction Poles initiated by Belgian Federal Office for Scientific, Technical and Cultural Affairs, X.G. by the National Fund for Scientific Research (FNRS-Belgium). A.P. acknowledges support from the Swiss National Science Foundation under Grant No. 620-57850.99. This study has also received financial support from the FRFC Project No. 2.4556.99. The calculations were performed on the NEC-SX4 and NEC-SX5 of the Swiss Center for Scientific Computing (CSCS) in Manno.

[1] G.D. Wilk and R.M. Wallace, Appl. Phys. Lett. **76**, 112 (2000); G.D. Wilk, R.M. Wallace, and J.M. Anthony, J. Appl. Phys. **87**, 484 (2000).

[2] W.-J. Qi, R. Nieh, E. Dharmarajan, B.H. Lee, Y. Jeon, L. Kang, K. Onishi, and J.C. Lee, Appl. Phys. Lett. **77**, 1704 (2000).

[3] F. Gervais, B. Piriou, and F. Cabannes, J. Phys. Chem. Solids **34**, 1785 (1973).

[4] W.B. Blumenthal, *The Chemical Behavior of Zirconium* (Van Nostrand, Princeton, 1958), pp. 201-219.

[5] Ph. Ghosez, J.-P. Michenaud, and X. Gonze, Phys. Rev. B **58**, 6224 (1998).

[6] P. Dawson, M.M. Hargreave, and G.R. Wilkinson, J. Phys. C **4**,

240 (1971).
[7] P. Hohenberg and W. Kohn, Phys. Rev. **136**, B864 (1964).
[8] W. Kohn and L.J. Sham, Phys. Rev. **140**, A1133 (1965).
[9] ABINIT is a common project of the Université Catholique de Louvain, Corning Incorporated, and other contributors (http://www.pcpm.ucl.ac.be/ABINIT). It relies on an efficient fast Fourier transform algorithm (Ref. 38) for the conversion of wave functions between real and reciprocal space, on the adaptation to a fixed potential of the band-by-band conjugate gradient method (Ref. 39) and on a potential-based conjugate-gradient algorithm for the determination of the self-consistent potential (Ref. 40). Technical details on the computation of responses to atomic displacements and homogeneous electric fields can be found in Ref. 20 while Ref. 21 presents the subsequent computation of dynamical matrices, Born effective charge tensors, dielectric permittivity tensors, and interatomic force constants.
[10] J.P. Perdew and Y. Wang, Phys. Rev. B **45**, 13 244 (1992).
[11] D.M. Ceperley and B.J. Alder, Phys. Rev. Lett. **45**, 566 (1980).
[12] M.P. Teter, Phys. Rev. B **48**, 5031 (1993).
[13] H.J. Monkhorst and J.D. Pack, Phys. Rev. B **13**, 5188 (1976).
[14] The calculations of the ground-state properties and of responses were also performed on a $2\times2\times2$ mesh of k points. The results obtained in both cases do not differ significantly, so we can consider that the convergence has been reached.
[15] Z. Mursic, T. Vogt, H. Boysen, and F. Frey, J. Appl. Crystallogr. **25**, 519 (1992).
[16] J.C. Nipko and C.-K. Loong, Physica B **241-243**, 415 (1998).
[17] J.-P. Crocombette and D. Ghaleb, J. Nucl. Mater. **257**, 282 (1998).
[18] The Brillouin zone for the body-centered-tetragonal lattice is the unit cell presented in Fig. 9(a) of G.F. Koster, *Solid State Physics: Advances in Research and Applications*, edited by H.E. Ehrenreich, F. Seitz, and D. Turnbull (Academic, New York, 1957), Vol. 5, pp. 173-276, rotated by 45°, to account for the passage from real to reciprocal space.
[19] X. Gonze, D.C. Allan, and M.P. Teter, Phys. Rev. Lett. **68**, 3603 (1992).
[20] X. Gonze, Phys. Rev. B **55**, 10 337 (1997).
[21] X. Gonze and C. Lee, Phys. Rev. B **55**, 10 355 (1997).
[22] W. Zhong, D. King-Smith, and D. Vanderbilt, Phys. Rev. Lett. **72**, 3618 (1994).
[23] F. Detraux and X. Gonze, Phys. Rev. Lett. **81**, 3297 (1998).
[24] C. Lee and X. Gonze, Phys. Rev. Lett. **72**, 1686 (1994).
[25] C. Lee, Ph. Ghosez, and X. Gonze, Phys. Rev. B **50**, 13 379 (1994).
[26] X. Gonze, J.-C. Charlier, D.C. Allan, and M.P. Teter, Phys. Rev. B **50**, 13 035 (1994).
[27] P. Giannozzi, S. de Gironcoli, P. Pavone, and S. Baroni, Phys. Rev. B **43**, 7231 (1991).
[28] C. Pecharromán, M. Ocaña, P. Tartaj, and C.J. Serna, Mater. Res. Bull. **29**, 417 (1994).
[29] X. Gonze, Ph. Ghosez, and R.W. Godby, Phys. Rev. Lett. **74**, 4035 (1995).
[30] R.M. Martin and G. Ortiz, Phys. Rev. B **56**, 1124 (1997).
[31] Ph. Ghosez, X. Gonze, and R.W. Godby, Phys. Rev. B **56**, 12 811 (1997).
[32] See, for example, J.P. Perdew, K. Burke, and M. Ernzerhof, Phys. Rev. Lett. **77**, 3865 (1996).
[33] Z.H. Levine and D.C. Allan, Phys. Rev. Lett. **63**, 1719 (1989).
[34] W.G. Aulbur, L. Jönsson, and J.W. Wilkins, Phys. Rev. B **54**, 8540 (1996).
[35] J.P. Perdew and M. Levy, Phys. Rev. Lett. **51**, 1884 (1983).
[36] L.J. Sham and M. Schlüter, Phys. Rev. Lett. **51**, 1888 (1983).
[37] A.A. Maradudin, E.W. Montroll, G.H. Weiss, and I.P. Ipatova, in *Solid State Physics: Advances in Research and Applications*, edited by H.E. Ehrenreich, F. Seitz, and D. Turnbull (Academic, New York, 1971), Suppl. 3, Chap. 4.
[38] S. Goedecker, SIAM J. Sci. Comput. (USA) **18**, 1605 (1997).
[39] M.C. Payne, M.P. Teter, D.C. Allan, T.A. Arias, and J.D. Joannopoulos, Rev. Mod. Phys. **64**, 1045 (1992).
[40] X. Gonze, Phys. Rev. B **54**, 4383 (1996).